The Development of an Intense East Asian Summer Monsoon Disturbance with Strong Vertical Coupling

C.-P. CHANG AND S. C. HOU*

Department of Meteorology, Naval Postgraduate School, Monterey, California

H. C. KUO AND G. T. J. CHEN

Department of Atmospheric Sciences, National Taiwan University, Taipei, Republic of China

(Manuscript received 30 April 1997, in final form 13 November 1997)

ABSTRACT

The East Asian summer monsoon (Mei-yu) disturbance of 17–25 June 1992 was the most intense 850-hPa low center of such systems during a 7-yr period. Due to the moisture fluxes associated with the southwesterlies from the warm tropical oceans, diabatic heating has generally been considered the main energy source of these heavy-precipitation disturbances as they propagate eastward from the eastern flank of the Tibetan Plateau across southeastern China and move into the East China Sea. In this study piecewise potential vorticity inversion is used to analyze the physical mechanisms of this intense case, particularly the possible roles of midlatitude baroclinic processes in its development and evolution.

The development of the low-level vortex involved the coupling with two upper-level disturbances, one at 500 hPa that also originated from the eastern flank of the Tibetan Plateau, and another at 300 hPa. Both disturbances appeared later than and upstream of the low-level vortex. Faster eastward movements allowed them to catch up with the low-level vortex and led to a strong vertical coupling and deep tropopause folding. Initially, diabatic heating was the dominant mechanism for the low-level vortex while the tropopause process opposed it. Both mechanisms supported the 500-hPa disturbance, and tropopause folding was the dominant mechanism for the 300-hPa disturbance. As the vertical coupling developed, the tropopause process reversed its earlier role in the low-level disturbance and contributed to its development. Boundary layer and adiabatic effects also became contributive as the disturbance moved out of eastern China to the oceanic region.

The vertical coupling of the three disturbances was a major factor in the development. The timing and position of the middle-tropospheric disturbance was critical in bridging the upper- and lower-level disturbances and a deep tropopause folding. This midlatitude-originated process compounded the diabatic heating effect that was sustained by tropical moist air, leading to the strong intensification.

1. Introduction

The East Asian summer monsoon starts in May (Tao and Chen 1987) and is marked with widespread low-level southwesterlies in Southeast Asia, southern China, and the tropical and subtropical western Pacific. These southwesterlies reach a low-level convergence zone on the northwestern periphery of the subtropical high, whose center is near the central Pacific. The convergence zone is along the East Asian summer monsoon trough, which often appears as a weak stationary front at the surface, with a modest temperature gradient but significant horizontal wind shear across it (Chen and Chang 1980). This zone is also a belt of frequent heavy rainfall that has been termed ''Mei-yu'' in China, ''baiu'' in Japan, and ''changma'' in Korea. Although there are intraseasonal variations in its location—usually a northward movement as the season progresses—in late spring and early summer the rain belt is usually quasi-zonally oriented near 30°N over eastern China and tilts east-northeastward toward Korea and Japan. The quasi-stationary front (the Mei-yu front in China, baiu front in Japan, and changma front in Korea) often extends from a cyclonic low center west-southwestward as the center itself moves eastward or east-northeastward. The heaviest rainfall is mostly associated with eastward-moving meso- to synoptic-scale disturbances along the front, and often in the low center itself.

Another heavy rain-producing and quasi-stationary phenomenon that is common during the East Asian summer monsoon is the low-level vortex that frequently develops on the eastern flank of the Tibetan Plateau (Tao

* Permanent affiliation: Department of Atmospheric Sciences, National Taiwan University, Taipei, Republic of China.

Corresponding author address: Prof. C.-P. Chang, Department of Meteorology, MR/Cp, Naval Postgraduate School, 589 Dyer Road, Room 254, Monterey, CA 93943-5114.
E-mail: cpchang@nps.navy.mil

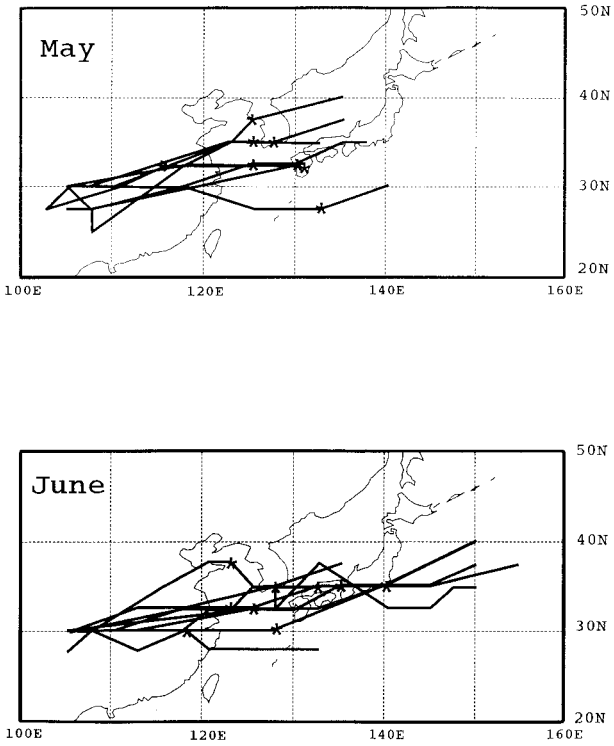

FIG. 1. Track of 850-hPa Mei-yu cyclone centers: (a) May and (b) June. For each track the location of the lowest height between 115° and 150°E is marked with a star.

and Ding 1981). These vortices appear to form as a result of the interaction between the topographic effect and the large-scale flow and receive most of their energy from latent heat release (e.g., Wu and Chen 1985; Kuo et al. 1986; Wang 1987; Wang and Orlanski 1987; Wang et al. 1993). In many cases, these vortices migrate eastward and become the cyclone centers for the Mei-yu front (Tao and Ding 1981; Ninomiya and Akiyama 1992).

A 7-yr climatology of the Mei-yu systems during May and June that are associated with the eastward migration of the Tibetan Plateau vortices is shown in Fig. 1. Here the tracks of the Mei-yu cyclone centers at 850 hPa during May and June of 1987–93 based on the European Centre for Medium-Range Weather Forecasts (ECMWF) analysis are plotted. A total of eight cases in May and nine cases in June during this 7-yr period is shown. For a case to be included, the cyclone center has to develop from inland southwestern China near 105°E and move out to the western Pacific east of 130°E. The location of the lowest 850-hPa height for each track is marked by a star in Fig. 1. The tracks themselves are not necessarily the location of the Mei-yu fronts because the latter often extend to the west-southwest from the centers.

Numerous observational and numerical studies showed that the low-level southwesterly transport of moisture from the tropical oceans, including the Bay of Bengal, the South China Sea, and the western Pacific, provide the major energy source in the form of latent heat for the development and maintenance of the disturbances in the Mei-yu rain belt (e.g., Ninomiya and Murakami 1987; Kuo et al. 1986; Wang 1987; Wang et al. 1993). In situ surface evaporation may also be an important source of moisture (Wang 1987). Climatologically, the baroclinic structure of the averaged Mei-yu front is shallow west of Japan, and becomes deep only east of about 135°E (Ninomiya and Akiyama 1992). Upper-tropospheric processes, such as the enhancement of vertical motion through a favorable upper-divergence pattern, are typically considered only secondary as a forcing mechanism for the Mei-yu system over eastern China. Among the few exceptions was a late May 1987 case reported by Chen and Li (1995). In this case an upper-level trough passage led to an upper-level horizontal deformation field, whose associated frontogenesis helped the lower-tropospheric warm and moist tongue to produce heavy precipitation.

TABLE 1. The 850-hPa height of the deepest Mei-yu cyclone center for each case during 1987–93. The 17–25 June 1992 case is the case for the present study.

Year	Dates	Height (m)	Dates	Height (m)
1987	18–26 May	1370		
1988	16–21 May	1380	18–24 June	1366
	18–26 May	1378		
1989	4–13 May	1372	4–10 June	1358
	25–30 May	1437		
1990			9–16 June	1421
1991	16–21 May	1422	6–16 June	1362
1992			11–15 June	1416
			15–20 June	1424
			17–25 June	1325*
1993	7–12 May	1395	1–6 June	1410
	16–24 May	1399	16–24 June	1355

The motivation of this study was to investigate the possible roles of upper-tropospheric processes, in comparison to other processes, in the development of the Mei-yu disturbances. Assuming that the significance of the upper-tropospheric process will be more evident in the stronger development cases, we chose the most intense case included in Fig. 1 for this study.

Table 1 lists the lowest 850-hPa height values for each case shown in Fig. 1. In general, the June cases tend to be more intense than the May cases, with five of the nine cases having central height less than or equal to 1366 m, lower than any of the May cases. The strongest case is 17–25 June 1992, which developed into one of the most intense Mei-yu systems ever observed in June when the cyclone moved out to the East China Sea. The life cycle of this disturbance that developed from the eastern edge of the Tibetan Plateau and propagated eastward to the western Pacific will be studied in this paper by analyzing its potential vorticity. We will use the diagnostic techniques of inverting the Ertel's potential vorticity with the nonlinear balance equation, designed by Davis and Emanuel (1991), to study the different

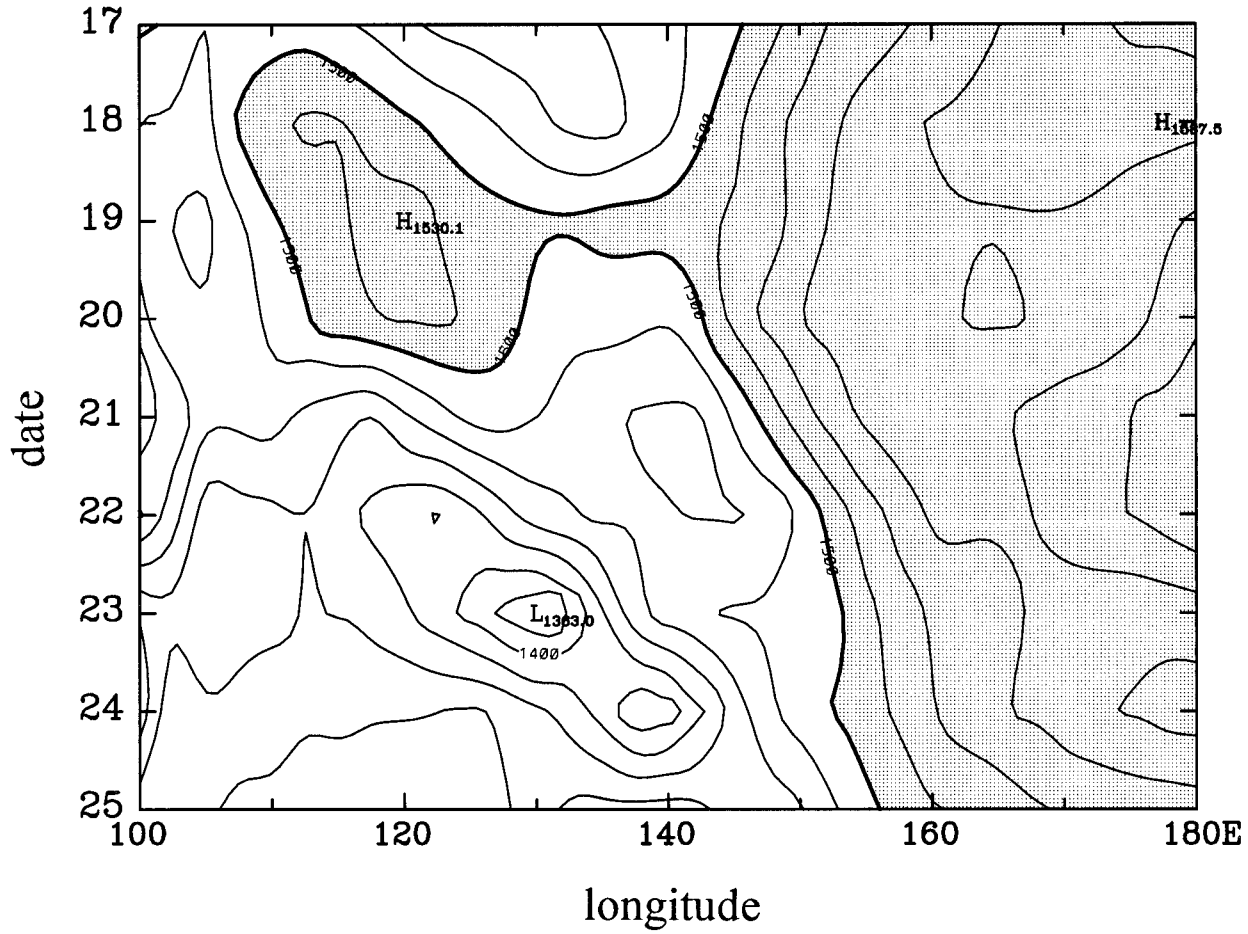

FIG. 2. Time–longitude section of 850-hPa height along 32.5°N for 17–25 June 1992. The interval is 20 m and the area higher than 1500 m is shaded.

roles played by the various physical processes in the development and evolution of this intense case. The results will demonstrate the crucial role played by the vertical coupling with separate middle- and upper-level midlatitude systems in the intensification of this disturbance. The most significant aspect of the vertical coupling is a tropopause folding, which appears to be responsible for the development of this most intense case in the 7-yr sample.

2. The synoptic case

The data used were the 0000 and 1200 UTC ECMWF analysis on 2.5° × 2.5° grids and seven pressure levels: 1000, 850, 700, 500, 300, 200, and 100 hPa, for the period 17–25 June 1992. Figure 2 is a time–longitude section of the 850-hPa height along 32.5°N in this period, which provides an overview of the eastward moving Mei-yu disturbance. The low center started around 0000 UTC 18 June 1992 near the western boundary of the diagram and moved slowly to the east for about two days along the edge of a northwestward extension of the subtropical high. As this extension was eroded, the disturbance penetrated rapidly eastward into the western Pacific. However, the western periphery of the main subtropical high as represented by the 1500-m contour retreated only slightly, and the high center near the date line appeared to remain stationary.

In the next three diagrams we will show the wind and geopotential height sequence at 850, 500, and 300 hPa, respectively. At each of these three levels, a disturbance appeared at different stages of this case, and eventually they developed a deep vertical coupling throughout the troposphere that played an important role in the intensification of the low-level Mei-yu disturbance. We will use A, B, and C to denote the lower-, middle- and upper-tropospheric systems, respectively. Figure 3 shows the time series of the 850-hPa wind and height at 0000 UTC for the entire period over the region 25°–40°N, 100°–160°E. The disturbance (labeled A first showed up at 0000 UTC 18 near 28°N, 105°E, which is approximately the eastern edge of the plateau at 850 hPa, and moved

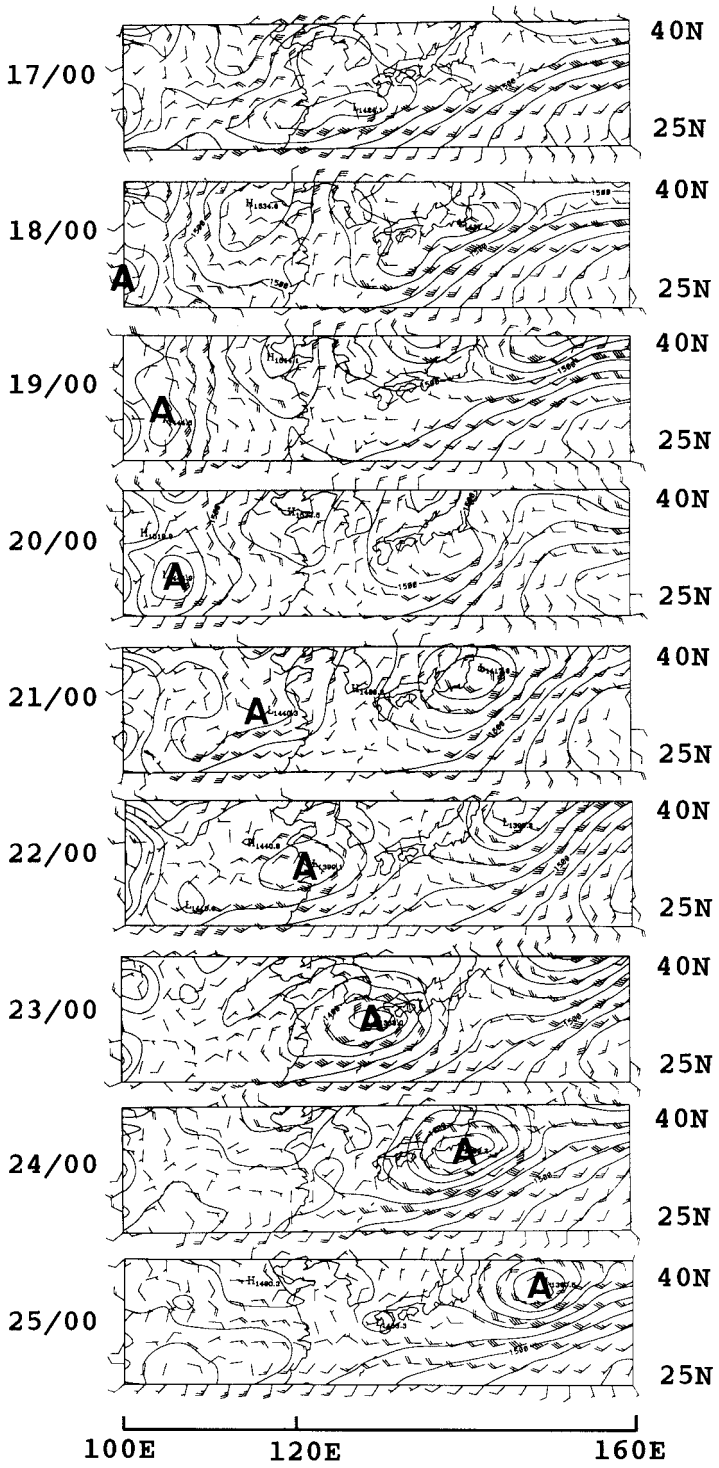

FIG. 3. The 850-hPa wind (full bar 5 m s^{-1}) and height (interval 20 m) between 25° and 40°N for 0000 UTC 17–25 June 1992. The center of the low-level disturbance is indicated by A.

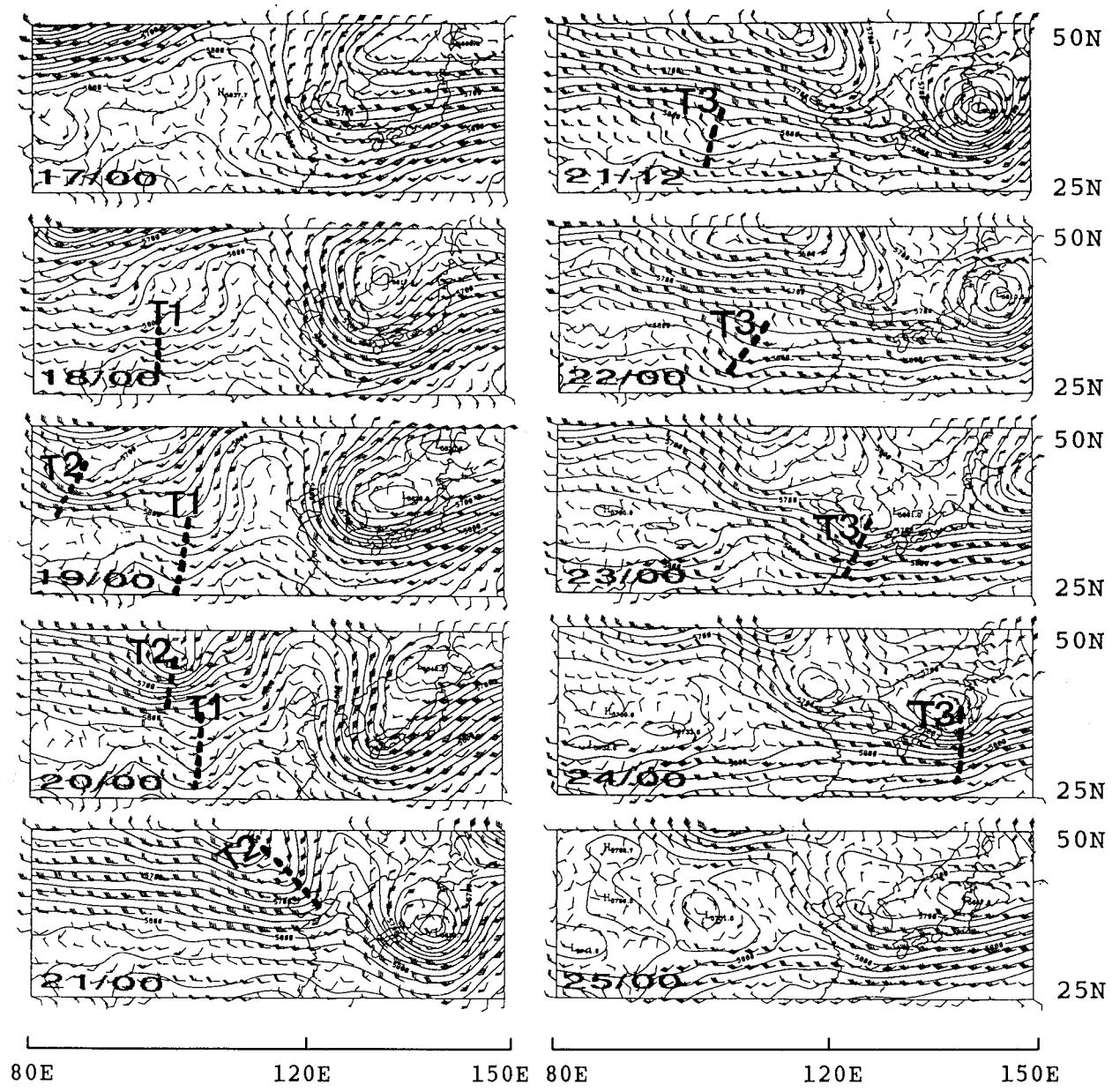

FIG. 4. The 500-hPa wind (full bar 5 m s^{-1}) and height (interval 20 m) between 25° and 50°N for 0000 UTC 17–25 June 1992, with the 1200 UTC 21 June diagram included. Here T1, T2, and T3 are trough lines discussed in the text, where T1 and T3 are related to disturbances A and B, respectively.

slowly eastward. After 21 June it appeared to split into two centers, with the main center moving rapidly eastward together with intensification. The maximum intensity was reached between 23 and 24 June near Japan, afterward it weakened in the western Pacific.

Figure 4 shows the wind and height at 500 hPa at 0000 UTC from 17 to 25 June (1200 UTC 21 June is also included). At 0000 UTC 18 June a lee trough (T1) appeared over the eastern edge of the plateau at 30°N, 98°E. This was a reflection of disturbance A at this level. At 0000 UTC 19 June this trough moved eastward with A while another trough (T2) appeared to the northwest north of 40°N and west of 90°E. The midlatitude trough had a faster eastward movement so that after 0000 UTC 20 June it caught up with the low-latitude trough, and the merged system swept eastward to reach 40°N, 120°E at 0000 UTC 21 June. This fast westerly movement implied a freshening of the westerly flow, which appears to be the reason the low-level disturbance A also moved to around 117.5°E at this time (Fig. 3). Meanwhile, a

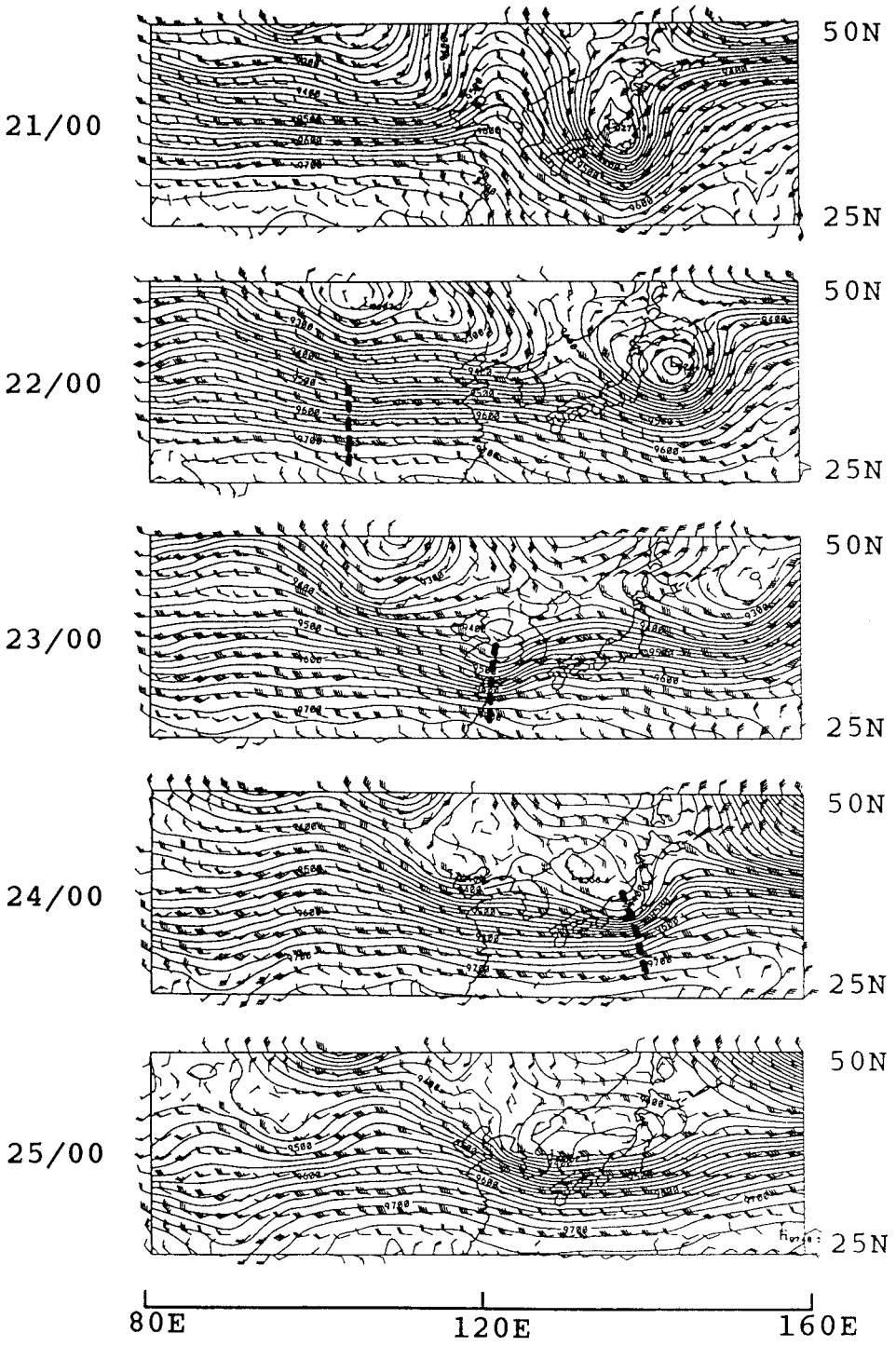

FIG. 5. The 300-hPa wind (full bar 5 m s^{-1}) and height (interval 20 m) between 25° and 50°N for 0000 UTC 21–25 June 1992. The upper-tropospheric disturbance (referred to as system C in the text) is indicated by a trough line.

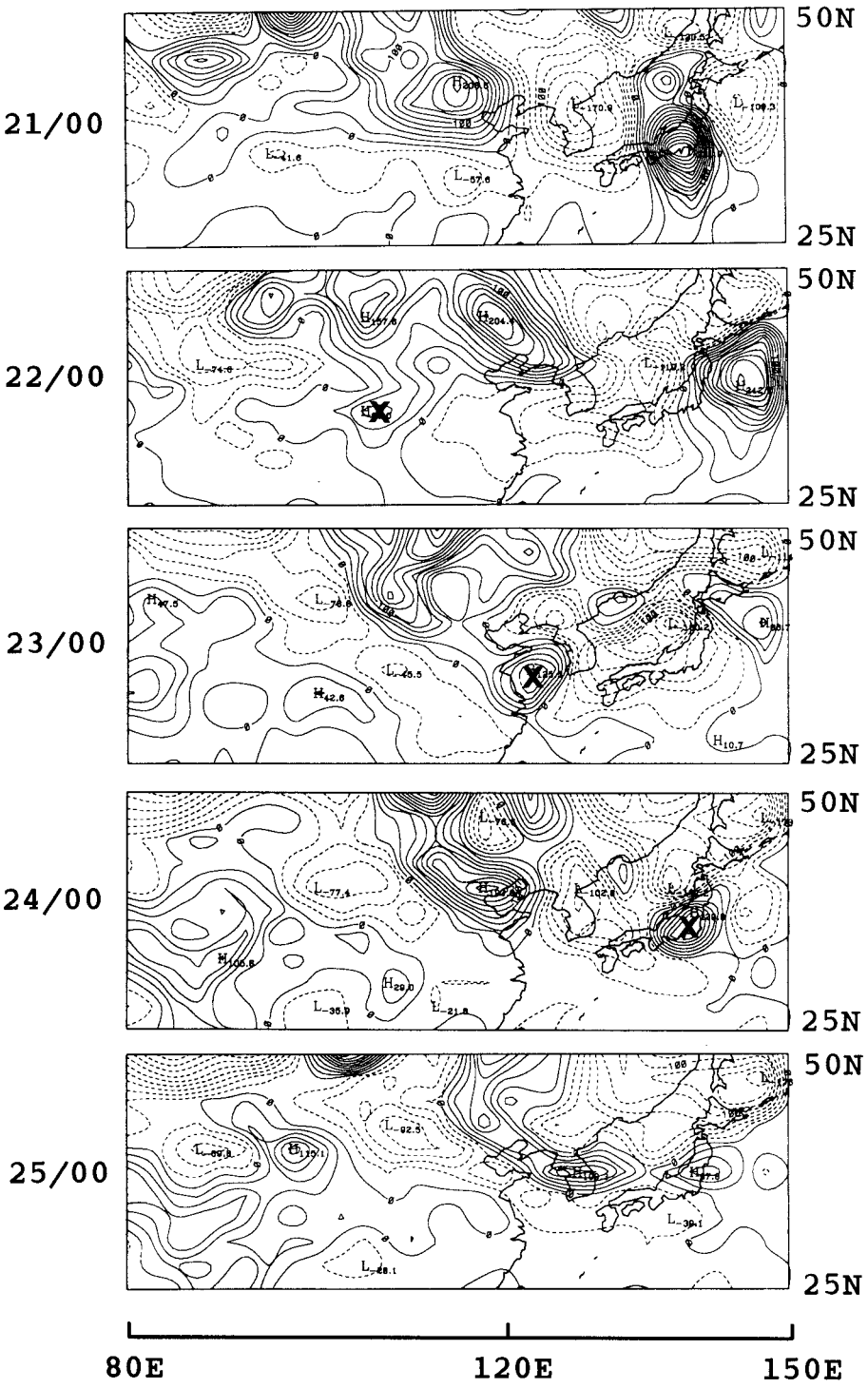

FIG. 6. The Ertel's potential vorticity perturbation (EPV′, interval 0.2 PVU) for 0000 UTC 21–25 June 1992 at 300 hPa. The center of the upper-tropospheric disturbance (system C) is marked.

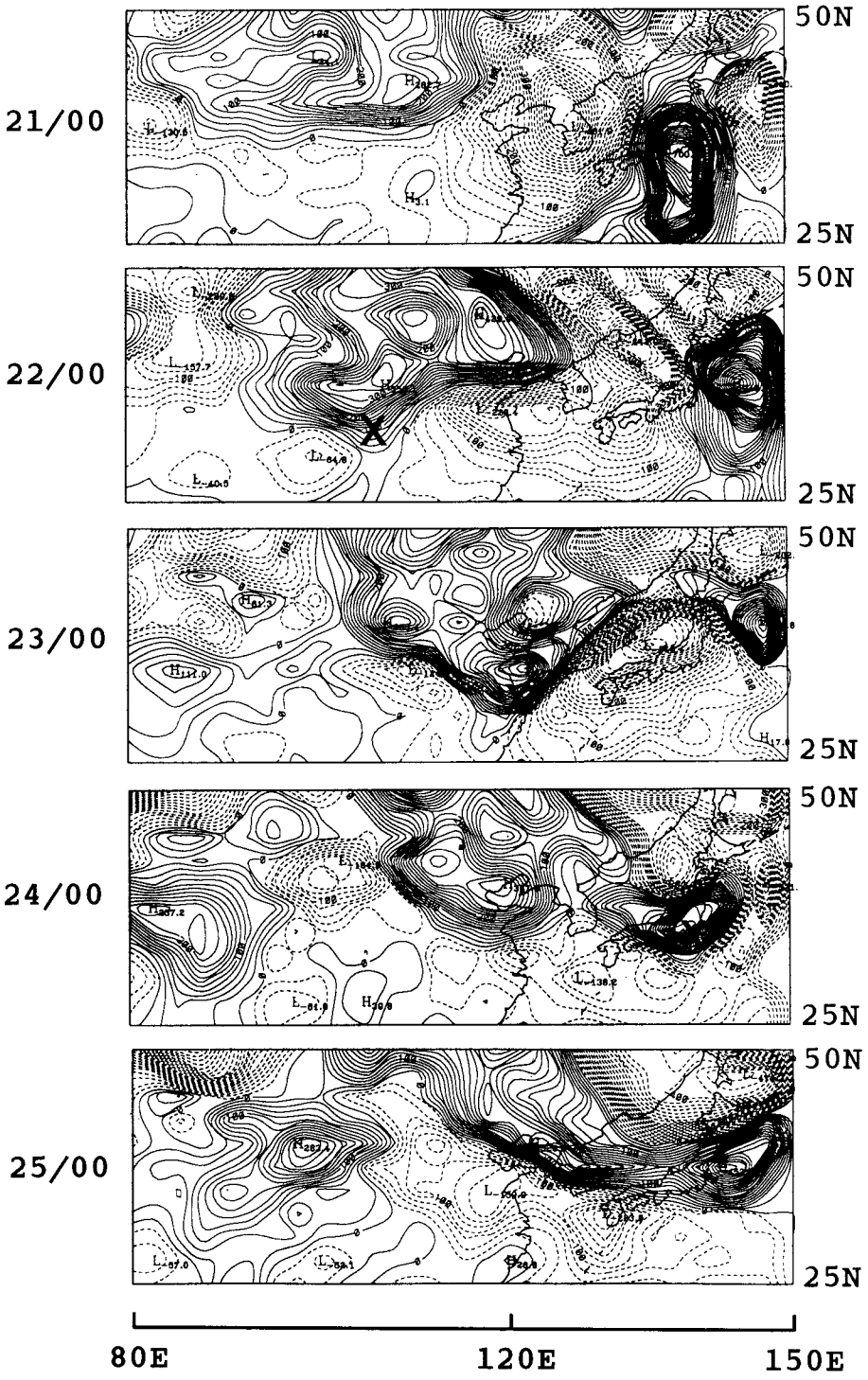

FIG. 7. Same as Fig. 6 except for 200 hPa. The location of the 300-hPa center of the upper-tropospheric disturbance (system C) is marked.

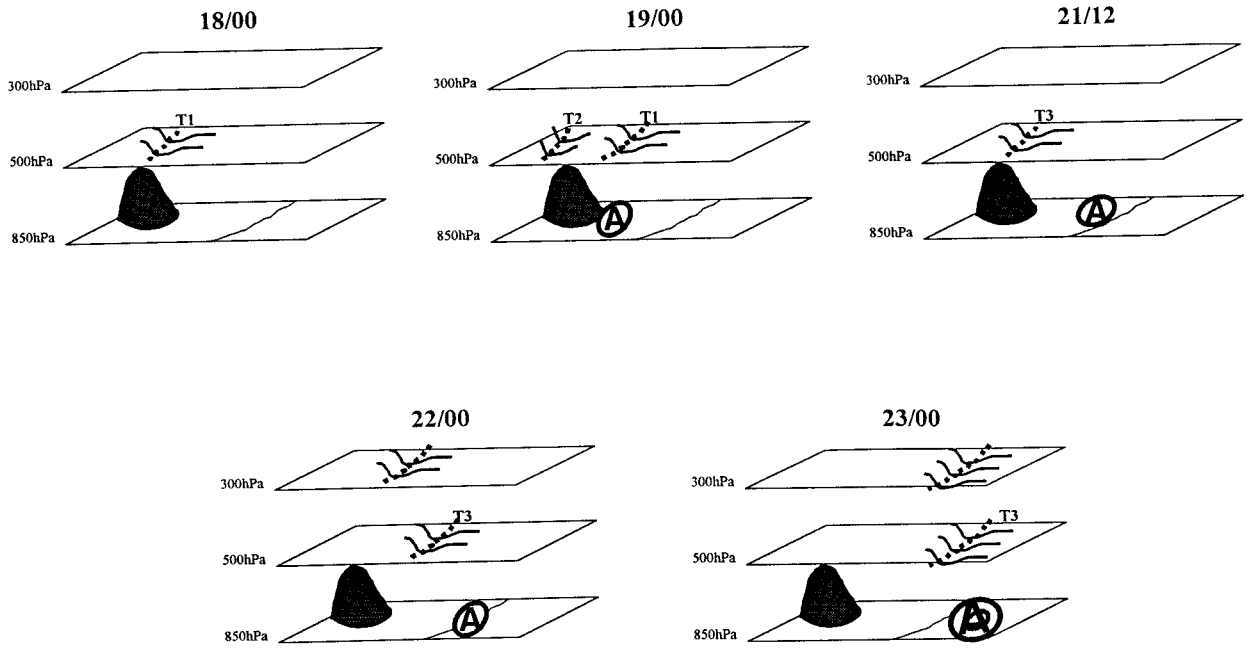

FIG. 8. Schematic diagram indicating the superposition of troughs at 500 hPa (where T3 is system B) and 300 hPa (system C) and the center of the 850-hPa disturbance (system A) at selected times. Time is indicated by DD/HH, where DD is the day in June and HH the UTC hour.

very weak 500-hPa trough that was barely visible appeared near 32.5°N, 102.5°E. This trough would become the middle-level disturbance B. It began to deepen 12 h later (marked as T3 in the 1200 UTC 21 June chart) and moved eastward to reach its maximum strength between 0000 UTC 23 June and 0000 UTC 24 June, when it became a cutoff low in the southern Sea of Japan. This was close to the location of the 850-hPa A center, which lay just to the south of the cutoff low.

Figure 5 shows the 300-hPa wind and height at 0000 UTC from 21 to 25 June. The upper-level disturbance C first appeared on 22 June as a trough near 30°N, 107.5°E (as indicated by east–west wind direction changes). It moved southeastward rapidly while deepening, reaching the vicinity of A and B on 0000 UTC 23 June. As will be shown later, the vertical coupling throughout the troposphere began at this time. The coupling lasted 24 h and the system became decoupled after 24 June.

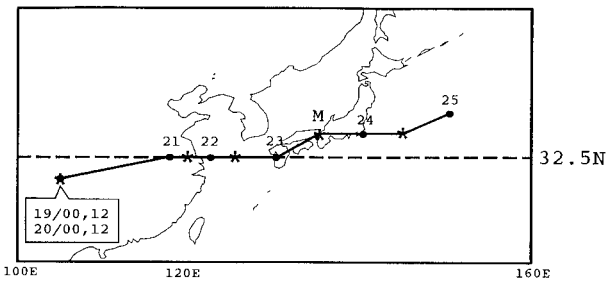

FIG. 9. Track of the center of the 850-hPa disturbance (system A). The dots represent 0000 UTC location and stars represent 1200 UTC location.

3. Height anomalies contributed by different physical processes

The significant deepening of the 300-hPa trough shown in Fig. 5 suggests that a tropopause folding process (Hoskins et al. 1985; Uccellini 1990) may play a role in the development. To examine this possibility, we computed the Ertel's potential vorticity (EPV), $q = (1/\rho)\boldsymbol{\eta}\cdot\nabla\theta$, where $\boldsymbol{\eta}$ is the absolute vorticity vector, θ the potential temperature, and ρ the density. The perturbations of EPV (EPV′, or q'), defined as the departure from the mean of the period 0000 UTC 17–23 June, at 300 and 200 hPa, are plotted in Figs. 6 and 7, respectively.

At 0000 UTC 22 June an isolated 300-hPa center of high EPV appeared around 32.5°N and 107.5°E (Fig. 6), the same location as the 300-hPa C trough shown in Fig. 5. There was no indication of this feature the previous day. This concentration of EPV′ strengthens throughout the next 48 h as it moved to the east coast of Japan at 0000 UTC 24 June, and disappeared at 0000 UTC 25 June. (The maximum value was reached at 1200 UTC 23 June, not shown.)

Unlike the isolated center at 300 hPa, the high q' at 200 hPa (Fig. 7) in the vicinity of the 300-hPa C trough appeared as an equatorward intrusion of the middle-

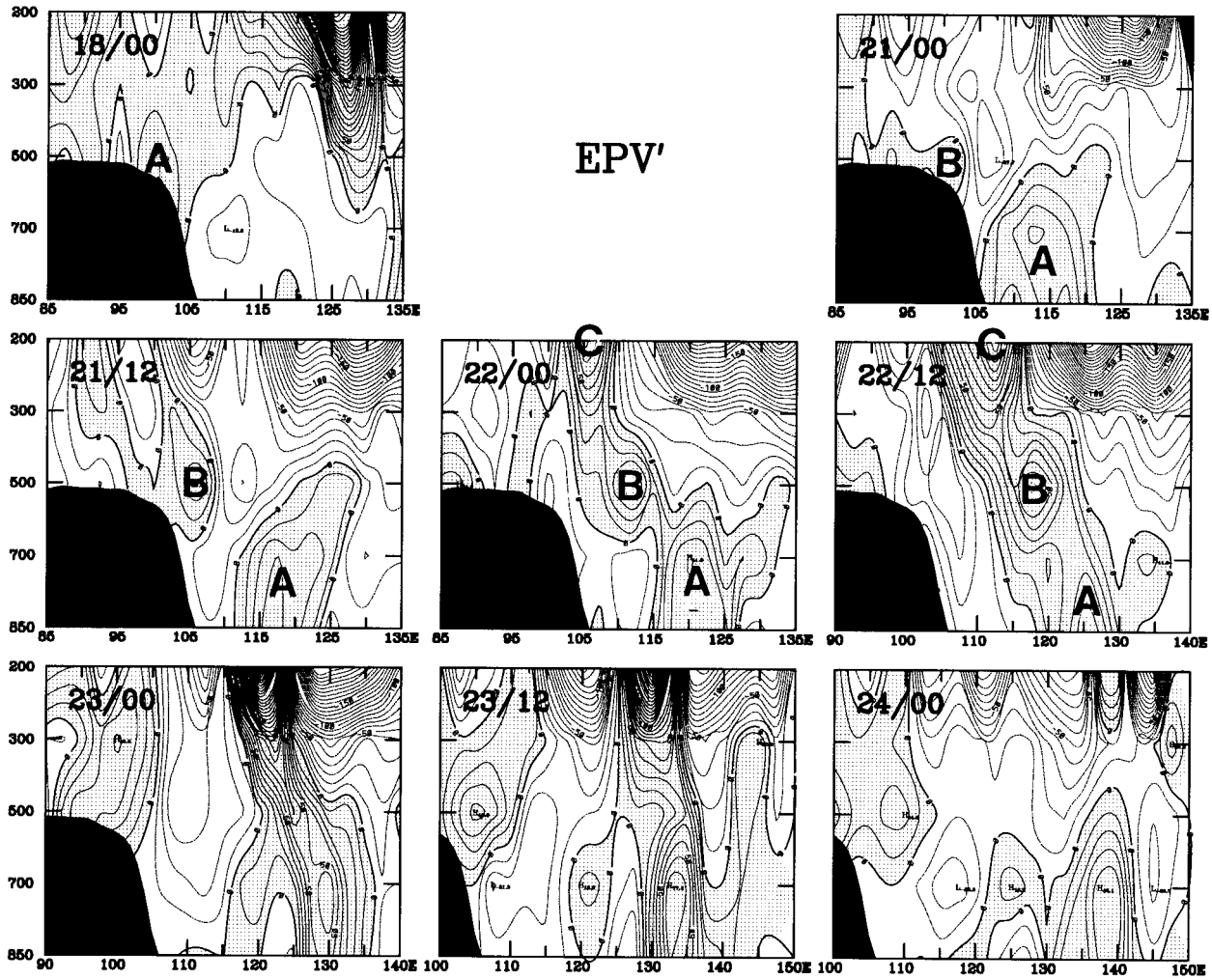

FIG. 10. Vertical (850–200 hPa) section of EPV′ (interval 0.1 PVU, positive area shaded) along 32.5°N for 0000 UTC 18 June and 0000 UTC 21 June to 0000 UTC 24 June with 12-h intervals. The longitudinal domain shifts with the disturbance center. The centers of the lower-, middle-, and upper-level disturbances are indicated by A, B, and C, respectively, prior to 0000 UTC 23 June when vertical coupling occurred.

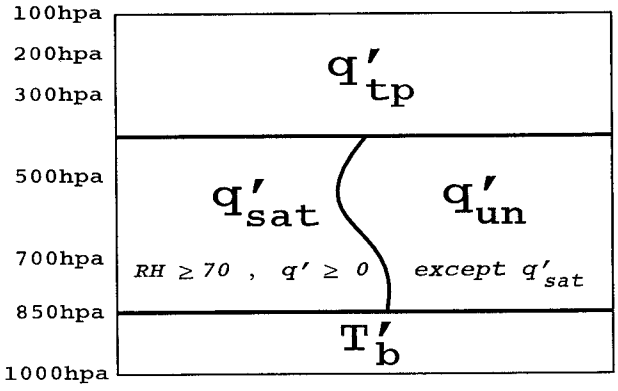

FIG. 11. Scheme for partitioning the total EPV′ for piecewise inversion to compute height anomalies contributed by different processes. Data levels are indicated by the pressure on the ordinate. See text for details.

latitude high EPVs. This high EPV′ sector, after ''spilling'' into the subtropics, continued to move eastward with the 300-hPa trough. Thus, the tropopause folding process is clearly originated from higher latitudes.

The positions of the troughs at 500, 300, and the 850-hPa A center at selected times are summarized schematically in Fig. 8. Here it shows that between 18–19 June the 500-hPa lee trough T1 moved eastward out of the Tibetan Plateau while the 850-hPa A center appeared at the eastern foothill. Here T1 dissipated and T2 moved northeastward out of the region when A moved to near the eastern coast on 1200 UTC 21 June. This was the time T3 (B) came out of the Tibetan Plateau. By 0000 UTC 22 June the tropopause folding began as was manifested by the appearance of a 300-hPa trough (C). The disturbances at the three levels lined up along an axis that tilted westward with height. All three moved eastward, with speeds increasing with height, so that by

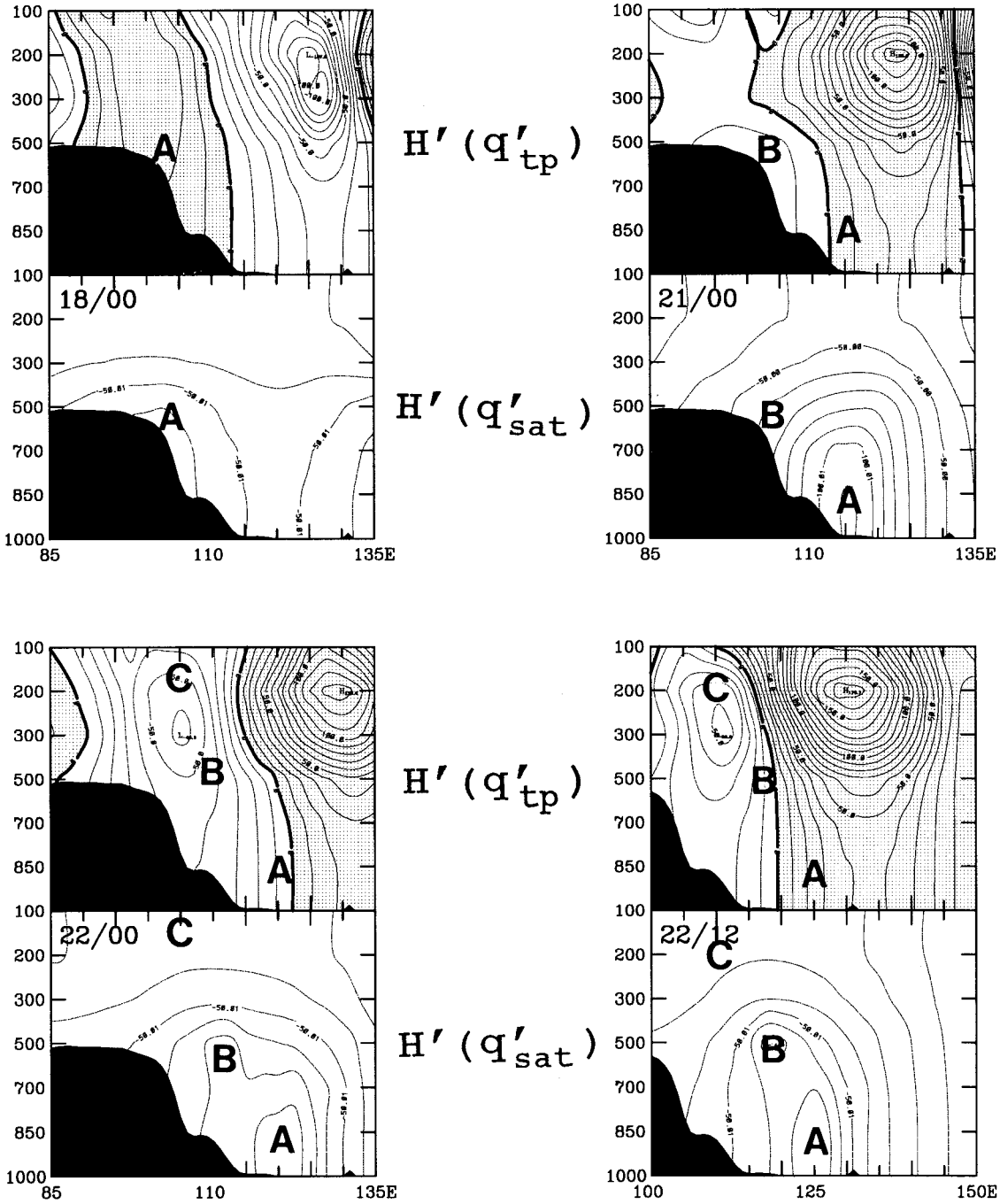

FIG. 12. The contributions of q'_{tp} (upper panels) and q'_{sat} (lower panels) to height anomaly (interval 10 m, positive values shaded) for the times indicated. The vertical coordinate is 1000–100 hPa.

0000 UTC 23 June the middle- and upper-level disturbances caught up with the lower-level center and resulted in a complete vertical coupling.

In the ensuing discussion, most of the diagrams will be along a longitude–height cross section along 32.5°N, which is close to the track of the 850-hPa center of the disturbance (Fig. 9). Figure 10 shows EPV′ along this cross section, at 0000 UTC 18 June and every 12 h from 0000 UTC 21 June to 0000 UTC 24 June. At 0000 UTC 18 June system A is observed near its initiating region on the eastern edge of the Tibetan Plateau. Between 1200 UTC 18 June and 1200 UTC 20 June (not shown) it moved down from 500 hPa along the eastern plateau slope. The split into two 850-hPa centers can be seen at 0000 UTC 21 June. At 0000 UTC 21 June, another disturbance (B) began to emerge on the eastern Tibetan

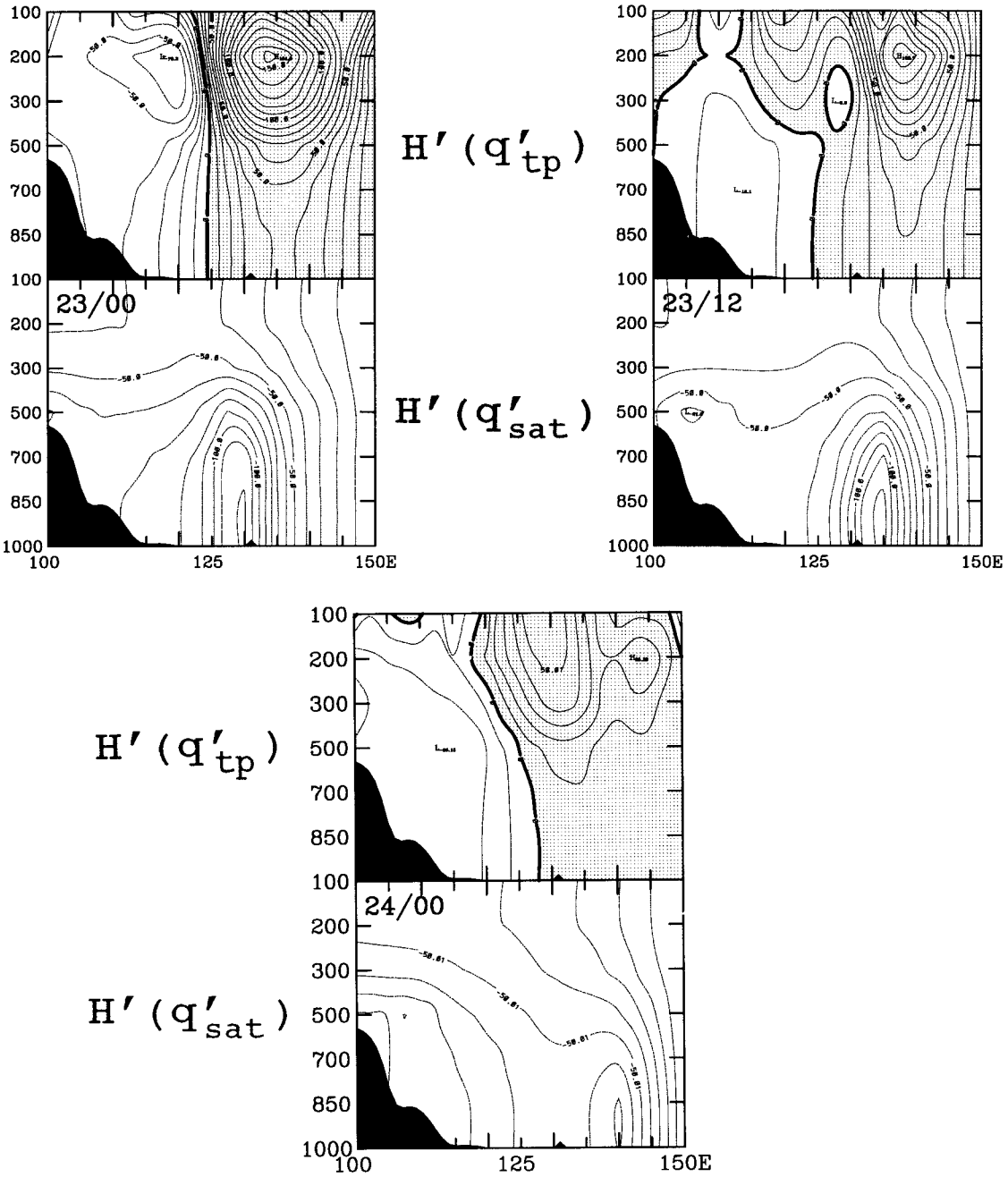

FIG. 12. (*Continued*)

Plateau. By 1200 UTC 21 June it moved eastward off the plateau while its center stayed near 500 hPa. Twelve hours later, at 0000 UTC 22 June a third disturbance (C) appeared above 300 hPa, while A at the lower level and B at the middle level continued their eastward movement. This was the time the tropopause folding, defined as a downward intrusion of the total EPV = 1.5 PVU (PV unit, 10^{-6} m^2 K kg^{-1} s^{-1}) isopleth into the troposphere (Hoskins et al. 1985), began. The three systems became vertically connected at 1200 UTC 22 June, when a positive EPV′ column, tilted slightly westward, encompassed all three disturbance centers. By 0000 UTC 23 June, the system showed the most organized vertical structure and the middle-tropospheric disturbance B lost its identity. This was the time that the vertical coupling throughout the troposphere and the strongest tropopause folding occurred. The maximum intensities of the low-level height anomaly and EPV′

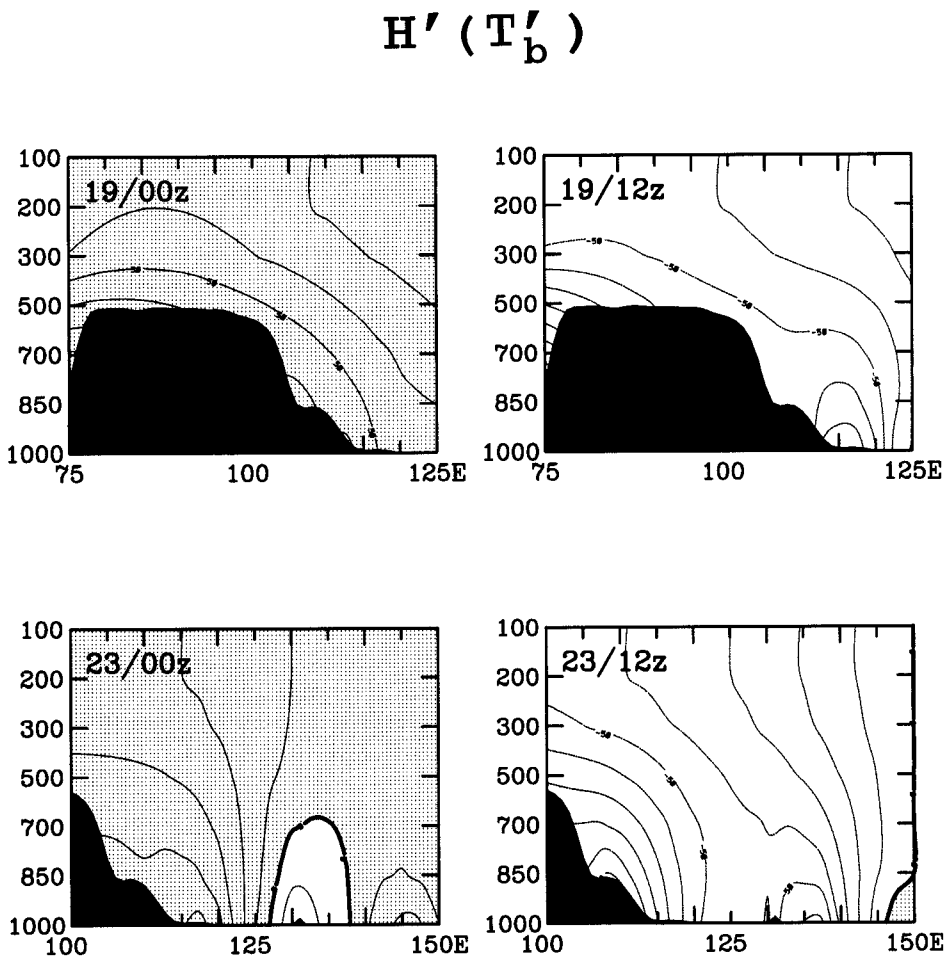

FIG. 13. As in Fig. 12 except for the contribution of boundary layer potential temperature anomaly to height anomaly for 0000 and 1200 UTC, 19 June and 23 June.

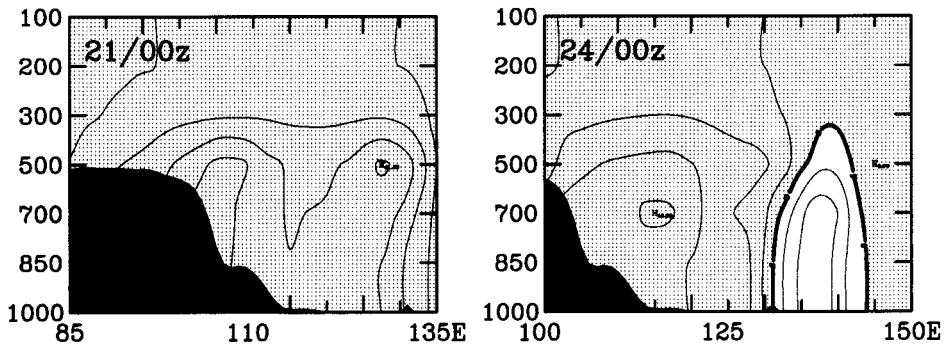

FIG. 14. As in Fig. 12 except for the contribution of q'_{un} to height anomaly for 0000 UTC 21 June and 0000 UTC 24 June.

were reached at 1200 UTC 23 June. At this time the vertical link began to decrease, and by 0000 UTC 24 June A was decoupled from upper levels.

To assess the effects of different physical processes in the evolution of the Mei-yu disturbance, we use Davis and Emanuel's (1991) piecewise EPV′ inversion technique by partitioning the EPV′ in the domain of study into several anomaly components to find the contribution of each component to the height anomaly (departure from period mean). Here the nonlinearity of the balance equation was handled in the same way as used in Davis and Emanuel's (1991)—that is, prescribing a ''pseudo mean'' for the geopotential height and streamfunction, which equals the mean value plus one half of the sum of the perturbation values at all points.

The partitioning method for this piecewise inversion followed the strategy used by Davis (1992b) and is shown schematically in Fig. 11. The effect of the EPV′ is divided into four parts: (a) the diabatic heating effect, which is represented by the EPV′ of nearly saturated [relative humidity (RH) $\geq$ 70%] high EPV ($q' \geq 0$) tropospheric (850–500 hPa) air, denoted by q'_{sat}; (b) the adiabatic effect of the unsaturated tropospheric air, whose EPV′ is denoted by q'_{un} which is the 850–500-hPa EPV′ other than q'_{sat}; (c) the tropopause effect (the effect that a higher tropopause potential vorticity tends to support a negative height perturbation in the column through the balance equation), represented by the EPV′ of air at 300 hPa and higher levels (q'_{tp}); and (d) the effect of boundary layer, as represented by the averaged 1000–850-hPa potential temperature anomaly (T'_b). The condition of $q' \geq 0$ in defining q'_{sat} is to identify only the condensation heating effect that produces positive vorticity.

The Tibetan Plateau area is affected by a strong diurnal cycle during northern summer, with maximum deep convection in the evening and minimum in the morning (Murakami 1983). The deep convection leads to large-scale divergent outflow in the upper troposphere near the tropopause. As a result, the upper levels also experience a diurnal effect that tends to raise the geopotential height in the evening and to lower it in the morning. This leads to a diurnal variation in the contribution to the height anomaly by the tropopause effect in the vicinity of the Tibetan Plateau, in that the morning (0000 UTC) contribution tends to favor negative height anomaly while the evening (1200 UTC) tends to favor positive height anomaly. These diurnal tendencies are strongest in the upper troposphere, but their influence can also penetrate to the lower levels. It should be noted, however, that this diurnal variation of the tropopause effect is of the opposite sign from the diurnal variation of the boundary layer effect, so that when both effects are considered, the diurnal tendency at the lower-tropospheric levels is dominated by the boundary layer effect.

Figure 12 compares the contributions of the height anomaly that are attributed to the tropopause (upper panel) and diabatic (lower panel) effects during selected stages of the disturbance. As may be expected, the diabatic effect always contributed to the negative height anomalies. At 0000 UTC 18 June (the initiation time of disturbance A when it developed near 500 hPa just off the eastern edge of the Tibetan Plateau) the maximum contribution of the diabatic heating effect was in the vicinity of A. This means the main diabatic effect was contributing to lower the height of A, therefore helping its development. In the meantime, the tropopause effect contributed to positive height anomalies in a deep column surrounding A, therefore it was clearly working against its development.

The two mechanisms maintained their respective effects on A through 0000 UTC 21 June, when the middle-level disturbance B first appeared on the eastern edge of the plateau. At this time the contribution for lowering the height from the diabatic heating effect has increased to the largest value since the genesis of A. The diabatic effect also contributed to the negative height anomaly surrounding B, with a slight indication of a local trough in the contribution diagram. The tropopause effect had a structure that was still working against A but it contributed to the lowering of height for B. Therefore, the development process for B was different from that for A, in that B was initiated both by diabatic heating and upper-level processes while A was entirely due to latent heating.

The upper-level disturbance C appeared 24 h later, at 0000 UTC 22 June. The diabatic heating effect at this time had two clearly defined local centers, contributing to both A and B. It had very little effect on C, signaling the fact that the development process for C was different from both A and B. The tropopause effect had a maximum contribution to negative height anomaly near C, and it was also helping B. In addition, this was also the first time the positive height anomaly column contributed by the tropopause effect moved outside of the A center, so that A was for the first time benefiting from the tropopause effect. This apparently marked a critical stage of the development as the three disturbance centers began the process toward a rapid vertical coupling. At 1200 UTC 22 June the tropopause process contributed to the upper-tropospheric development of the disturbance and the diabatic heating contributed to the middle- and lower-level development. It may be noted that at this time the lower disturbance center was again in the region of positive height anomaly contributed by the tropopause effect. This is a manifestation of the diurnal variation of the tropopause effect discussed earlier.

The vertical structure of the coupled system became most organized throughout the troposphere at 0000 UTC 23 June,[1] when the coupling was complete, and the three

[1] At this time the tropopause contribution appeared slightly opposed to the disturbance at low levels, but this was misleading. The positive

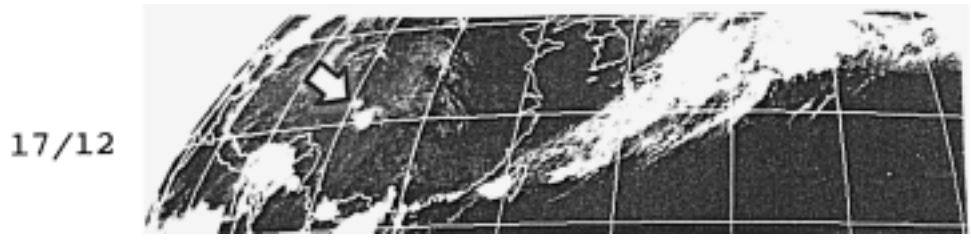

FIG. 15. GMS satellite infrared images for 1200 UTC 17 June and 0000 UTC 19–24 June.

separate disturbances may be considered as one system (Fig. 10). Twelve hours later, the contribution of the diabatic effect reached a maximum, which was responsible for the occurrence of maximum intensity at 850 hPa. The tropopause contribution can be seen both in a negative height anomaly around 300 hPa, and a local reduction of the positive (due to the period mean, see footnote 1) anomaly at the 850-hPa center near 119°E. The latter implies that the low-level pressure was falling as the cyclone center approached. Both effects weakened at 0000 UTC 24 June, when the 850-hPa disturbance, whose center has moved to 140°E, collapsed to a shallow system below 500 hPa.

As mentioned before, the effect of the boundary layer (as represented by T'_b) had strong diurnal variations, with the morning (0000 UTC) opposing the 850-hPa low and the evening (1200 UTC) contributing to it. This contrast is clearly indicated when comparing the effect between 0000 and 1200 UTC 19 June (Fig. 13). However, when the system moved over the ocean, even the morning effect was contributing to the low, as shown at 0000 and 1200 UTC 23 June (Fig. 13). In addition to the fact that the diurnal effect over water is much reduced, the strong surface winds will facilitate sensible and latent heat fluxes from the ocean.

The effect of the unsaturated air (represented by q'_{un}) generally opposed the low with positive anomalies over the disturbance. This is shown in the example for 0000 UTC 21 June in Fig. 14. This was the case throughout the life of the disturbance until 0000 UTC 24 June, when it became contributive to the low-level low system[2] (Fig. 14). Figure 15 shows the sequence of 0000 UTC satellite images for 19–24 June, preceded by the 1200 UTC 17 June image (because 0000 UTC 18 June was missing). System A was in the formation stage on 1200 UTC 17 June when it showed up as a small cloud cluster in the satellite image. It migrated slowly eastward until 0000 UTC 21 June when it began the rapid eastward movement. System B appeared at 1200 UTC 21 June (not shown) and system C appeared at 0000 UTC 22 June. They combined as one large organized cloud band behind another that was associated with A on 0000 UTC 22 June. The two cloud bands merged on 0000 UTC 23 June as the vertical coupling developed. The system continued to move eastward over the western Pacific but the cloudy area shrank considerably on 0000 UTC 24 June. This may explain the substantial contribution from q'_{un} to the disturbance as a large area of the cyclonic disturbance was under clear conditions.

4. Height tendency and vertical motion

In this section we used the nonlinearly balanced flow from the EPV to compute the height tendency and vertical pressure velocity (omega) fields, as was done by Davis and Emanuel (1991). Again, the purpose was to elucidate the roles played by different physical processes. In section 3 the height anomalies were calculated in a linear framework, where the summation of the responses from the four physical processes equals exactly the total disturbance structure. However, the sign of the instantaneous anomaly depends directly on the choice of the period mean, or events before and after the given time, so that a misleading sign may appear (see footnote 1). In this section the height tendency is calculated nonlinearly and brings out more readily the instantaneous tendency implied in the linear results, but the summation of all contributions may not equal to the total. These two approaches complement each other in providing cross-checks in the results.

For this purpose the set of prognostic equations involved is highly nonlinear and special procedures are required to evaluate an individual process. Following Davis (1992b), the height tendency and omega associated with the effect of a particular EPV anomaly were estimated by subtracting those computed without this effect from the results of the total EPV. This procedure corresponds to the ''ST'' method described in Davis (1992a), and is but one of many possible approaches in distributing the nonlinear interactions of different anomalies; the choice of approach is necessarily arbitrary. Davis' (1992b) work showed that although interactions of different EPV anomalies may cause some ambiguity in the interpretation of the results, useful and qualita-

height anomaly shown in Fig. 12 was an artificial result of the choice of the period for computing mean. If a preceding strong tropopause folding event (without a coupled low-level system, visible in the upper-right corner of the 0000 UTC 18 June panel of Fig. 10) was excluded from the period, a negative height anomaly will surround the disturbance.

[2] At this time the cyclone center has moved to 35°N, north of the cross section. The result there shows an even stronger q'_{un} contribution to the low center than indicated in Fig. 14.

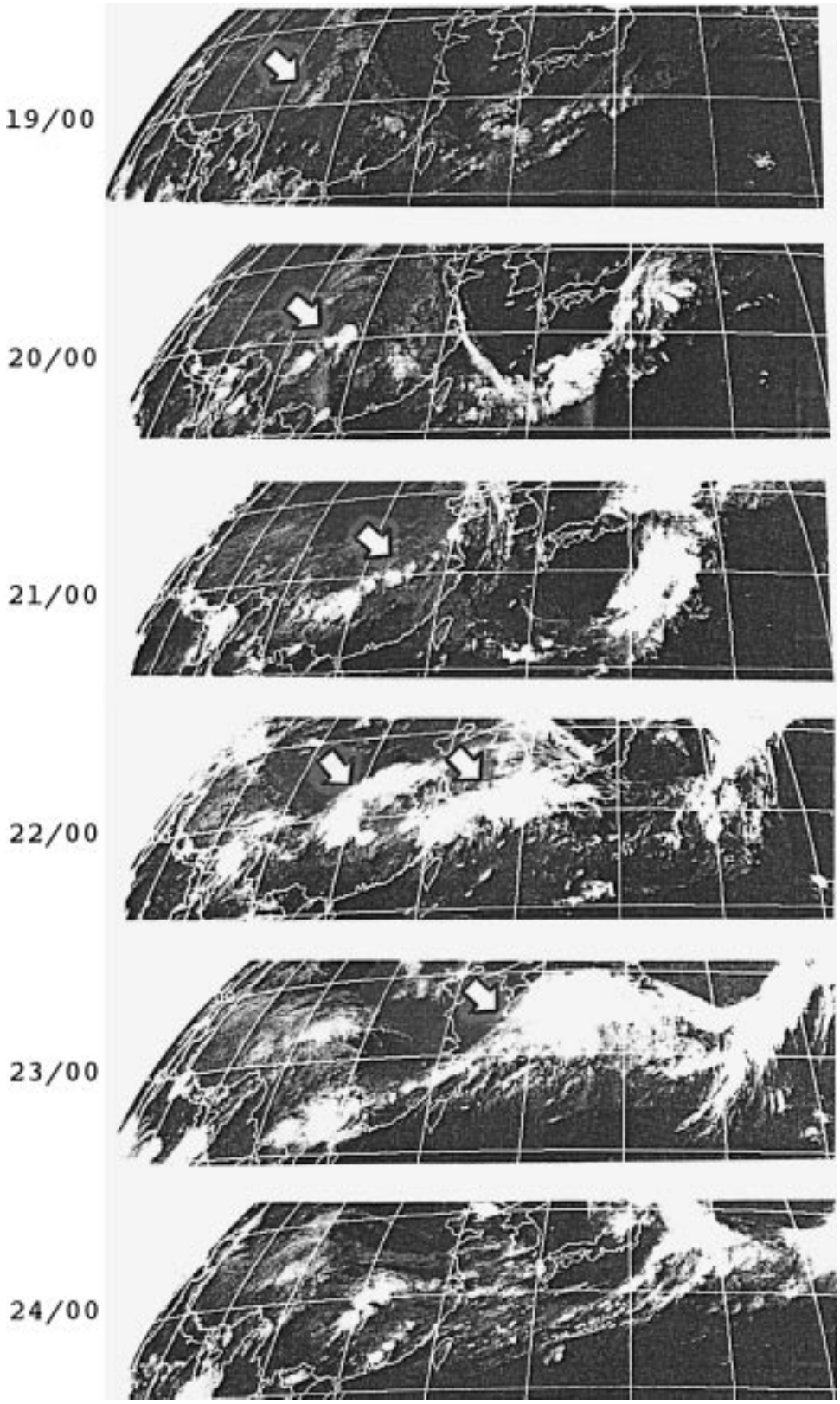

FIG. 15. (*Continued*)

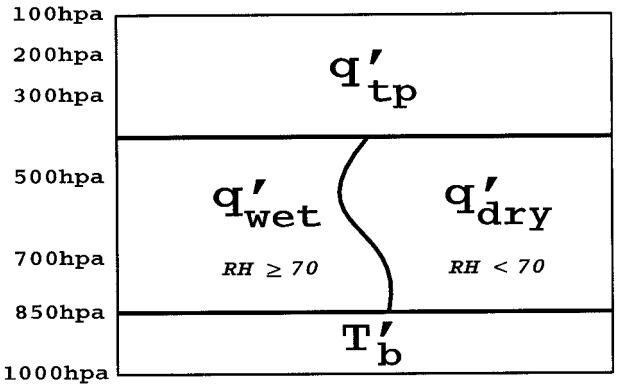

FIG. 16. Scheme for partitioning the total EPV′ for height tendency and omega calculations. Data levels are indicated by the pressure on the ordinate. See text for details.

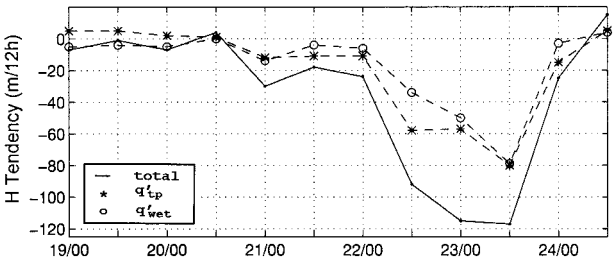

FIG. 17. Nonlinearly balanced height tendency [m (12 h)$^{-1}$] at the 850-hPa low center associated with total (solid), q'_{tp} (dash-*), and q'_{wet} (dash–circle).

tively reliable results can be obtained with this approach. To reduce the ambiguity related to the diabatic effect, we chose a slightly different scheme to partition the EPV′, as shown in Fig. 16. Here the free tropospheric (850–500 hPa) EPV′ is partitioned into a diabatic anomaly (q'_{wet}) whose sole condition is RH is equal to or greater than 70% regardless of the sign of q', and an unsaturated anomaly (q'_{dry}) where RH is less than 70%. The tropopause (q'_{tp}) and boundary layer (T'_b) effects are defined the same ways as those in the piecewise inversion for height anomalies.

In Fig. 17 the total instantaneous nonlinear height tendency following the 850-hPa A center is compared with those due exclusively to q'_{tp}, and q'_{wet}, if each acts alone. The values are given as change per 12 h. These two anomalies provide similar forcing of the height tendency and their sum nearly explains the total through 0000 UTC 23 June, when the tendency was near maximum. Afterward the sum exceeds the total as the latent heat release and the tropopause folding were both so intense that, in the absence of other processes, additional nonlinear effects occurred.[3] Both effects quickly diminished on 0000 UTC 24 June, the time of the vertical decoupling, and became detrimental to the disturbance 12 h later.

Figure 18 shows the total nonlinear height tendency for the cross section along 32.5°N and that associated with q'_{tp} and q'_{wet} at three selected synoptic times. At 1200 UTC 19 June, the lower-troposphere total tendency downstream of system A was negative, corresponding to the eastward movement of A from the edge of the plateau. At that time the tendency due to q'_{tp} was positive while that due to q'_{wet} was negative. This suggests that the tropopause effect was opposing the actual tendency while the latent heat effect was reinforcing it. At 0000 UTC 23 June, the starting time of the vertical coupling, the tendency of q'_{tp} was negative and had a center at 1000 hPa. Although this center did not completely coincide with the surface center of the total tendency, the tropopause effect was clearly contributing to the low-level height tendency. The tendency of q'_{wet} was in good agreement with the total. By 1200 UTC 23 June, q'_{tp} and q'_{wet} tendency centers both coincided with the total tendency center. This was the time that contribution from the tropopause air to the lowering of the 850-hPa height center reached a maximum, which was consistent with the fact that this was the time A reached maximum intensity.

The total nonlinearly balanced vertical motion and those calculated from q'_{tp}, q'_{wet}, and q'_{dry} at five selected times are shown in Fig. 19. At 1200 UTC 18 June the total vertical velocity was upward, as were those due to q'_{wet} and q'_{dry}, but the vertical motion due to q'_{tp} was downward, again indicating that in the initial stage the tropopause effect opposed the development. By 0000 UTC 22 June, the time of the first appearance of the upper-level system C, the tropopause effect was clearly upward and nearly represented the total upward motion. At this time both q'_{wet} and q'_{dry} gave very little vertical motion. Twelve hours later, the tropopause effect remained important for the rising motion of B and C, and the effect of moisture resumed its substantial contribution to the rising motion at A, apparently because A had moved over the East China Sea. These two effects appeared to give rise to the two rising motion centers shown in the total omega. The drier air continued to play very little role in the vertical motion field.

By 0000 UTC 23 June, the moist air exerted increased effect and gave rise to an upward motion center in the same position as the total center. This was the beginning of vertical coupling as the fast eastward movement of B and C caught up with A, and the tropopause effect interacted with the moisture effect. The mutual adjustment of these two effects brought the two previous upward motion centers together. The upward motion reached a maximum at 1200 UTC 23 June when all

[3] It is possible to force the sum of the four anomaly effects to equal to the total solution by a weighted average of the ''AM'' and ''ST'' anomaly solutions described by Davis (1992a), with the AM solution given three times the weight of the ST solution. However, this is itself arbitrary and there is no reason to expect that the distribution of the interactive terms in this way is better.

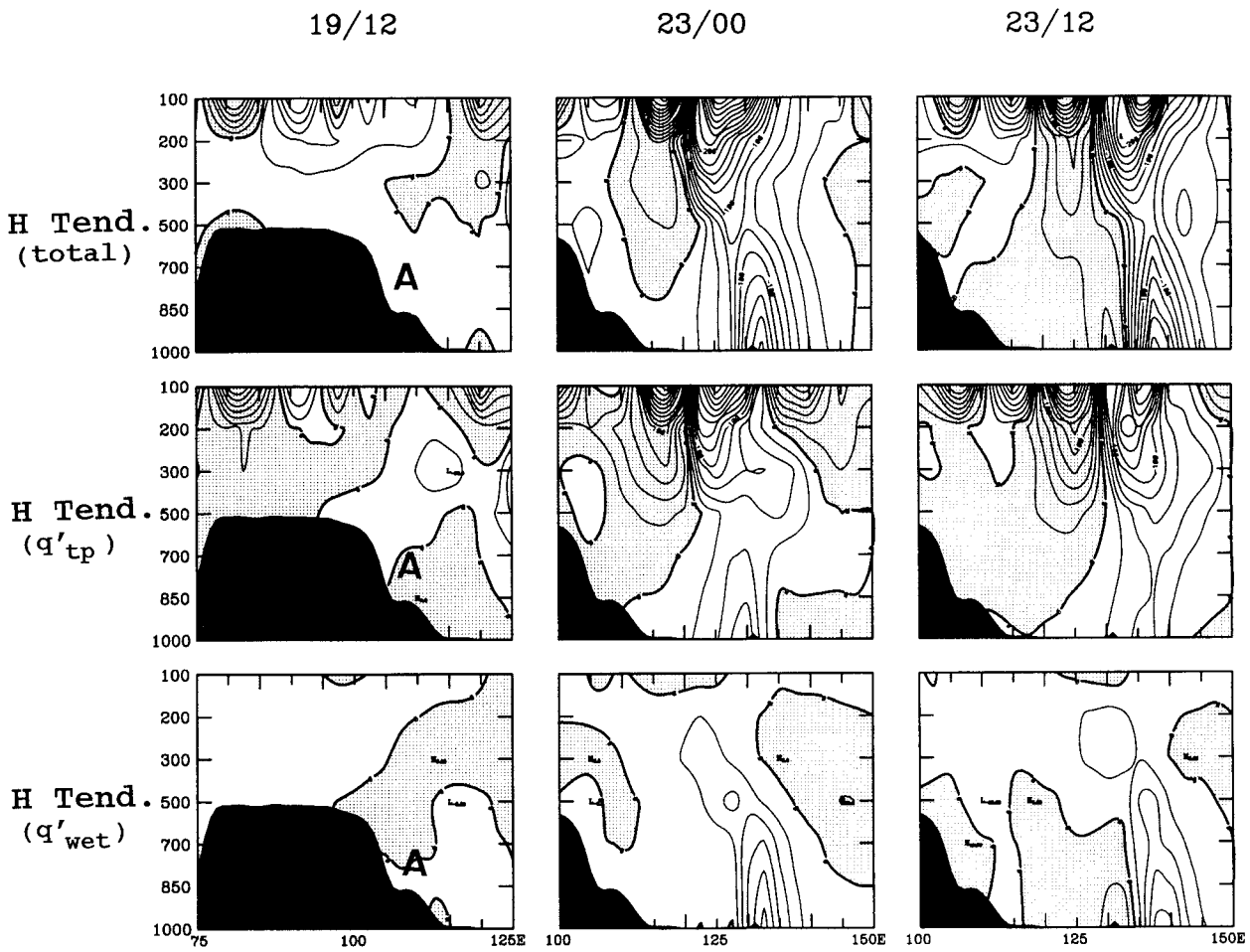

FIG. 18. The height tendency [interval 20 m (12 h)$^{-1}$] associated with total (top), q'_{tp} (middle), and q'_{wet} (bottom), for 1200 UTC 19 June, 0000 UTC 23 June, and 1200 UTC 23 June. The position of disturbance L is marked on the 1200 UTC 19 June charts.

effects, including that due to the drier air, gave similar patterns with centers in all panels coinciding.

5. Summary and concluding remarks

In this study we examined the Mei-yu case of 18–24 June 1992, looking for reasons that it produced one of the most intense synoptic-scale low centers at 850 hPa during the East Asian monsoon. The track of this center was typical of many similar Mei-yu cyclones. It started from a low-level vortex that originated at the eastern flank of the Tibetan Plateau and migrated east-northeastward to Korea, Japan, and the western Pacific. In this case the vortex became vertically coupled with two other disturbances, one in the middle troposphere near 500 hPa and the other at the tropopause, both of which developed a few days later in the upstream region but caught up with the low-level vortex as they moved rapidly from the eastern coastal region of China to Korea, Japan, and the surrounding oceans. The vertical coupling deepens the tropopause folding extensively and appeared to contribute significantly to the intensification of this Mei-yu center.

We used the diagnostic technique of piecewise potential vorticity inversion of the nonlinear balance equation developed by Davis and Emanuel (1991) to evaluate the roles played by diabatic, adiabatic, tropopause, and boundary layer processes. The techniques involve a certain degree of arbitrariness to resolve the problem of the nonlinearity, particularly in the prognostic equations. Previous studies by Davis and others showed that the problem of this arbitrariness is not serious and will not affect the results qualitatively.

The resultant height anomalies indicate that at their respective initial stages the development of the low-level disturbances was supported by diabatic heating, the middle-level disturbance by both diabatic heating and tropopause processes, and the upper-level disturbance by tropopause folding alone. Diabatic heating was extremely important for the low-level vortex initially when the tropopause process was detrimental to its development. However, with the development of the mid-

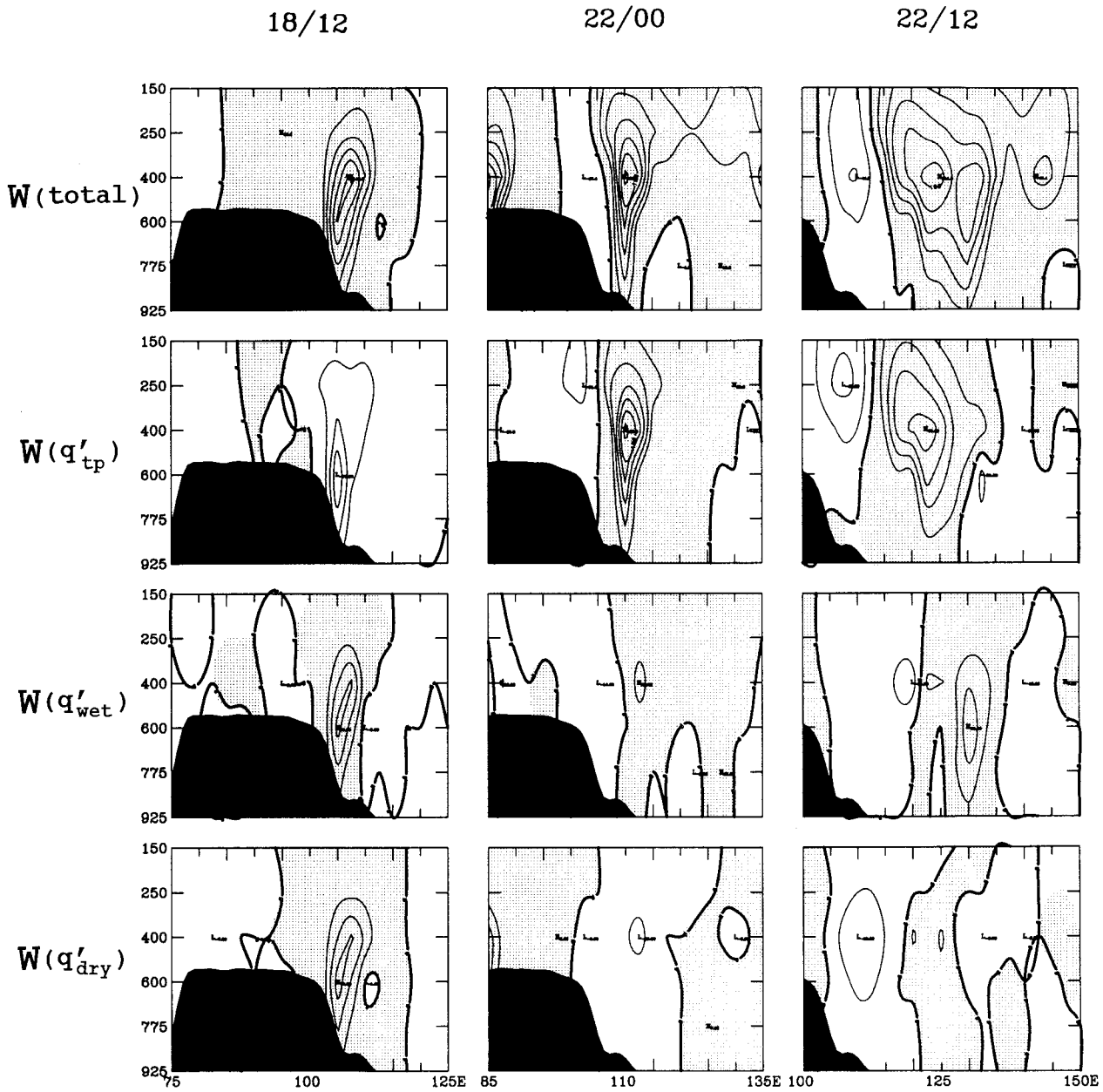

FIG. 19. Vertical (925–150 hPa) section of vertical velocity (interval 2 cm s^{-1}) associated with total (top), q'_{tp} (upper middle), q'_{wet} (lower middle), and q'_{dry} (bottom), for 1200 UTC 18 June, 0000 UTC 22 June, 1200 UTC 22 June, 0000 UTC 23 June, and 1200 UTC 23 June.

dle- and upper-level disturbances the effect of the tropopause changed to become favorable to the low-level disturbance. This took place when the vertical coupling began to occur. The disturbance intensity reached a maximum soon after the vertical structure became the most organized throughout the entire troposphere. These results were supported by the height tendency and vertical velocity produced by the different anomaly fields.

The strong vertical coupling through the troposphere and lower stratosphere was an important factor in the development of this Mei-yu disturbance. Thus, in addition to the diabatic process, which may be considered a tropical process as most of the warm and moist air is transported by the southwesterly monsoon winds, the midlatitude baroclinic process may also play an important role in the East Asian summer monsoon. However, this strong vertical coupling was not observed in all cases. It appeared that the occurrence of the middle-tropospheric disturbance (B) in this case played a critical role. It filled the gap between the lower-tropospheric and the tropopause disturbances and facilitated the vertical coupling and tropopause folding. We draw this conclusion both from examining the life cycle of this case and from analyzing other cases in the 7-yr dataset. We

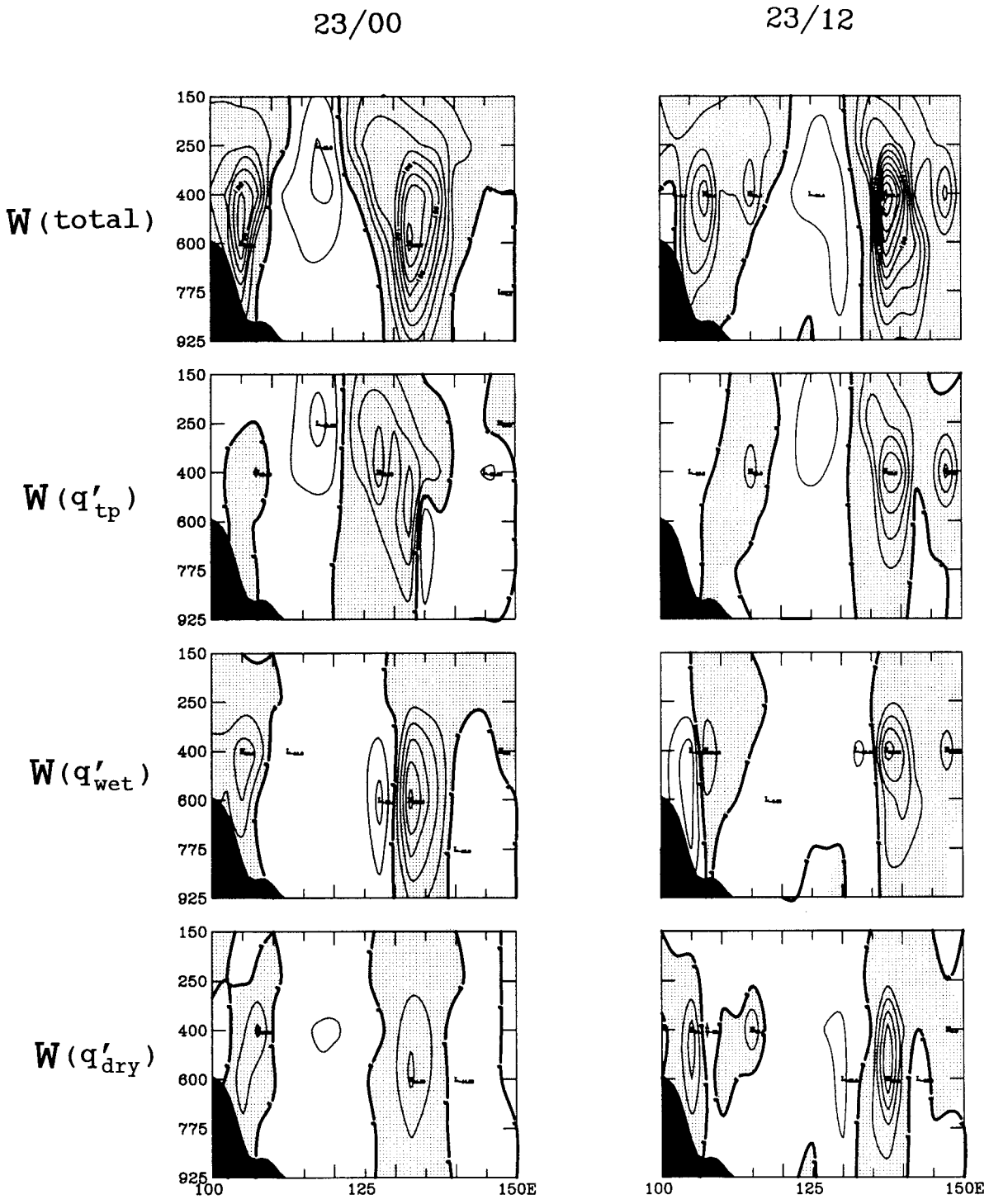

FIG. 19. (*Continued*)

are in the process of assessing the roles of different mechanisms in all the cases within the 1987–95 period with the piecewise EPV inversion diagnostics, the results will be reported elsewhere.

In addition to the Mei-yu systems that developed as a result of the eastward migration of the vortices that originated near the eastern flank of the Tibetan Plateau, two other types of Mei-yu disturbances have been observed during the East Asian summer monsoon. The Mei-yu rain belt can develop as a result of a midlatitude cold front that moves southward over eastern China and Korea, Japan, and adjacent seas. This front extends from

a midlatitude cyclone at its eastern or northeastern end and often connects with a topographically produced vortex on the Tibetan Plateau flank at its western end. In this type of Mei-yu front the plateau-induced vortex remains nearly stationary, and the front tends to have a more extensive zonal extent than the type studied in this paper. Another type of Mei-yu rainfall system may develop from a low-level low center that started in southern China, without involving the Tibetan Plateau vortices. Only when all these types are studied can we obtain a more complete picture of the mechanisms of the heavy rainfall disturbances associated with the East Asian summer monsoon.

Acknowledgments. We are indebted to Dr. Chris Davis for kindly making his potential vorticity diagnostic program available. We also wish to thank him and Dr. Paul Hirschberg for providing invaluable help in using the program, and Dr. Pat Pauley for reading the manuscript. This work was supported by the National Science Foundation Grants ATM 9525755 and ATM 9613746, and by the Office of Naval Research, Marine Meteorology Program.

REFERENCES

Chen, G. T.-J., and C.-P. Chang, 1980: The structure and vorticity budget of an early summer monsoon trough (Mei-Yu) over southeastern China and Japan. *Mon. Wea. Rev.*, **108,** 942–953.

Chen, Y.-L., and J. Li, 1995: Large-scale conditions favorable for the development of heavy rainfall during TAMEX IOP3. *Mon. Wea. Rev.*, **123,** 2978–3002.

Davis, C. A., 1992a: Piecewise potential-vorticity inversion. *J. Atmos. Sci.*, **49,** 1397–1411.

——, 1992b: A potential-vorticity diagnosis of the importance of initial structure and condensational heating in observed extratropical cyclogenesis. *Mon. Wea. Rev.*, **120,** 2409–2428.

——, and K. A. Emanuel, 1991: Potential vorticity diagnostics of cyclogenesis. *Mon. Wea. Rev.*, **119,** 1929–1953.

Hoskins, B. J., M. E. McIntyre, and A. W. Robertson, 1985: On the use and significance of isentropic potential-vorticity maps. *Quart. J. Roy. Meteor. Soc.*, **111,** 877–946.

Kuo, Y.-H., L. Cheng, and R. A. Anthes, 1986: Mesocale analyses of the Sichuan flood catastrophe, 11–15 July 1981. *Mon. Wea. Rev.*, **114,** 1984–2003.

Murakami, T., 1983: Analysis of the deep convective activity over the western Pacific and Southeast Asia. Part I: Diurnal variation. *J. Meteor. Soc. Japan*, **61,** 60–75.

Ninomiya, K., and T. Murakami, 1987: The early summer rainy season (Baiu) over Japan. *Monsoon Meteorology*, C.-P. Chang and T. N. Krishnamurti, Eds., Oxford University Press, 93–121.

——, and T. Akiyama, 1992: Multiscale feature of Baiu, the summer monsoon over Japan and East Asia. *J. Meteor. Soc. Japan*, **70,** 467–495.

Tao, S.-Y., and Y.-H. Ding, 1981: Observational evidence of the influence of the Qinghai Xizang (Tibet) Plateau on the occurrence of heavy rain and severe convective storms in China. *Bull. Amer. Meteor. Soc.*, **62,** 23–30.

——, and L. X. Chen, 1987: A review of recent research of the East Asian summer monsoon in China. *Monsoon Meteorology*, C.-P. Chang and T. N. Krishnamurti, Eds., Oxford University Press, 60–92.

Uccellini, L. W., 1990: Processes contributing to the rapid development of extratropical cyclones. *Extratropical Cyclones: The Erik Palmen Memorial Volume*, C. W. Newton and E. O. Holopainen, Eds., Amer. Meteor. Soc., 81–105.

Wang, B., 1987: The development mechanism for Tibetan Plateau warm vortices. *J. Atmos. Sci.*, **44,** 2978–2994.

——, and I. Orlanski, 1987: Study of a heavy rain vortex formed over the eastern flank of the Tibetan Plateau. *Mon. Wea. Rev.*, **115,** 1370–1393.

Wang, W., Y. H. Kuo, and T. T. Warner, 1993: A diabatically driven mesoscale vortex in the lee of the Tibetan Plateau. *Mon. Wea. Rev.*, **121,** 2542–2561.

Wu, G. X., and S. J. Chen, 1985: The effect of mechanical forcing on the formation of a mesoscale vortex. *Quart. J. Roy. Meteor. Soc.*, **111,** 1049–1070.